9. A. C. Newton and D. E. Koshland, Jr., *ibid.* **262**, 10185 (1987).
10. Y. A. Hannun *et al.*, *ibid.* **260**, 39 (1985).
11. L. Petruzzelli, R. Herrera, O. M. Rosen, *Proc. Natl. Acad. Sci. U.S.A.* **81**, 3327 (1984); M. F. White, H.-U. Haring, M. Kasuga, C. R. Kahn, *J. Biol. Chem.* **259**, 255 (1984); M. A. Shia, J. B. Rubin, P. F. Pilch, *ibid.* **258**, 14450 (1983).
12. R. Rangel-Aldao and O. M. Rosen, *J. Biol. Chem.* **251**, 7526 (1976).
13. T. M. Lincoln, D. A. Flockhart, J. D. Corbin, *ibid.* **253**, 6002 (1978).
14. J. Kuret and H. Schulman, *ibid.* **260**, 6427 (1985).
15. A unique Nde I site was created at the initiator ATG of the PKC βII gene by site-directed mutagenesis. An Nde I–Bam HI fragment was cloned into pAR3040 to optimally align the gene behind a strong T7 phage promoter and Shine-Dalgarno sequence. Transformants of BL21 containing the resulting plasmid were examined for protein kinase C activity after induction with isopropyl-β-D-galactopyranoside.
16. P. J. Parker *et al.*, *Science* **233**, 853 (1986).
17. J. L. Knopf *et al.*, *Cell* **46**, 491 (1986).
18. K. P. Huang, H. Nakabayashi, F. L. Huang, *Proc. Natl. Acad. Sci. U.S.A.* **83**, 8535 (1986).
19. N. Dedner, H. E. Meyer, C. Ashton, G. F. Wildner, *FEBS Lett.* **236**, 77 (1988).
20. J. R. Woodgett and T. Hunter, *J. Biol. Chem.* **262**, 4836 (1987).
21. C. House, R. E. H. Wettenhall, B. E. Kemp, *ibid.*, p. 772.
22. G. Hardie, *Nature* **335**, 592 (1988).
23. C. House and B. E. Kemp, *Science* **238**, 1726 (1987).
24. A. Kishimoto *et al.*, *J. Biol. Chem.* **264**, 4088 (1989).
25. M. D. Summers and G. E. Smith, *A Manual of Methods of Baculovirus Vectors and Insect Cell Culture Procedures* (Texas Agriculture Experiment Station, College Station, TX, 1987).
26. T. Uchida and C. R. Filburn, *J. Biol. Chem.* **259**, 12311 (1984).
27. U. Kikkawa *et al.*, *FEBS Lett.* **223**, 212 (1987).
28. Y. Ono *et al.*, *Proc. Natl. Acad. Sci. U.S.A.* **86**, 4868 (1989).
29. L. Coussens *et al.*, *Science* **233**, 859 (1986).
30. J. A. Cooper, B. M. Sefton, T. Hunter, *Methods Enzymol.* **99**, 387 (1983).
31. We thank the Howard Hughes Medical Institute and A. Admon for his expertise in peptide sequencing; J. Knopf for the full-length rat PKCII cDNA; M. Summers for the baculovirus starter kit; and H. Biemann for recommending the phosphatidylserine affinity matrix. Supported by NIH grant DK09765 and NSF grant 840200.

12 March 1990; accepted 25 May 1990

Four-Dimensional Heteronuclear Triple-Resonance NMR Spectroscopy of Interleukin-1β in Solution

Lewis E. Kay, G. Marius Clore, Ad Bax, Angela M. Gronenborn

A method is presented that dramatically improves the resolution of protein nuclear magnetic resonance (NMR) spectra by increasing their dimensionality to four. The power of this technique is demonstrated by the application of four-dimensional carbon-13–nitrogen-15 (^{13}C-^{15}N)–edited nuclear Overhauser effect (NOE) spectroscopy to interleukin-1β, a protein of 153 residues. The NOEs between NH and aliphatic protons are first spread out into a third dimension by the ^{15}N chemical shift of the amide ^{15}N atom and subsequently into a fourth dimension by the ^{13}C chemical shift of the directly bonded ^{13}C atoms. By this means ambiguities in the assignment of NOEs between NH and aliphatic protons that are still present in the three-dimensional ^{15}N-edited NOE spectrum due to extensive chemical shift overlap and degeneracy of aliphatic resonances are completely removed. Consequently, many more approximate interproton distance restraints can be obtained from the NOE data than was heretofore possible, thereby expanding the horizons of three-dimensional structure determination by NMR to larger proteins.

OVER THE LAST FEW YEARS IT HAS been shown that two-dimensional (2D) NMR spectroscopy (*1*) can be used to determine the solution structures of small proteins (≤100 residues) at a resolution comparable to that attainable by x-ray crystallography (*2–4*). The initial stage in an NMR structure determination involves spectral assignment by means of experiments that demonstrate through-bond and through-space correlations (*5*). The principal source of geometric information resides in short (<5 Å) approximate interproton distance restraints derived from NOE experiments, and the accuracy and precision of an NMR structure determination depends critically on the number of restraints that can be extracted from the data (*3, 4*). The application of 2D NMR methods to larger proteins has been impeded by two factors. First, the increase in the number of resonances leads to severe chemical shift overlap and degeneracy, rendering the assignment of through-bond interactions or through-space interactions or both increasingly difficult. Second, the increase in molecular weight results in larger linewidths so that the sensitivity of through-bond correlation experiments based on small (<12 Hz) homonuclear couplings is much reduced.

Many of the uncertainties present in 2D NMR spectra can be resolved by spreading out the 2D spectra into a third dimension (*6*), and NMR techniques based on large heteronuclear couplings should permit applications to larger proteins (*7*). To this end a number of three-dimensional (3D) heteronuclear NMR experiments that rely on large resolved heteronuclear couplings have been developed (*8–13*) and have been shown to be highly efficient for spectral assignment of proteins labeled with ^{15}N or ^{13}C or both up to a molecular weight of about 20 kD (*14*). Despite this added resolution, ambiguities still remain in the interpretation of 3D heteronuclear NMR spectra of larger proteins, so that an additional increase in resolution afforded by raising the dimensionality still further is desirable. In this paper we report a four-dimensional (4D) NMR experiment and demonstrate its applicability to uniformly labeled ^{15}N-^{13}C interleukin-1β (IL-1β), a 17.4-kD protein of 153 residues, that plays a central role in the immune and inflammatory responses (*15*).

All 2D NMR experiments comprise four distinct steps, namely, preparation, evolution, mixing, and detection (*16*). A 4D NMR experiment is easily conceived by combining three 2D NMR experiments, leaving out the detection period of the first, the preparation and detection periods of the second, and the preparation period of the third. The 4D experiment we have chosen to perform is one in which NOEs between NH protons and aliphatic protons are spread out by the chemical shifts of the directly bonded ^{15}N and ^{13}C atoms, respectively. The rational behind this experiment lies in resolving extensive ambiguities still present in a 3D ^{15}N-edited NOESY experiment (3D ^1H-^{15}N NOESY-HMQC) in which NOEs between NH protons and aliphatic protons are spread into the third dimension by the chemical shift of the directly bonded ^{15}N atoms (*8, 9*). Although this 3D experiment effectively removes, in all but a very few cases, chemical shift degeneracy associated with the NH protons, it leaves the ambiguities associated with severe overlap of aliphatic resonances unaffected. Thus, even if a cross peak connecting an aliphatic and amide proton is well resolved in the 3D spectrum, it is frequently not possible, with the exception of cases involving the CαH resonances, to identify conclusively the aliphatic proton involved on the basis of its ^1H chemical shift.

The progression and relation between ^{15}N-^{13}C–heteronuclear-edited 2D, 3D, and 4D NOESY experiments is illustrated schematically in Fig. 1. In the 2D spectrum, NOEs between NH protons (F_2 dimension) and aliphatic protons (F_1 dimension) are

observed in a single plane. In the 3D spectrum, these NOEs are spread within a 3D cube over a series of $F_3(NH)$-$F_1(^1H)$ slices according to the chemical shift of the directly bonded ^{15}N atoms in the F_2 dimension. In the 4D experiment, each slice at a particular ^{15}N frequency of the 3D spectrum constitutes a cube within the 4D spectrum in which each cube is subdivided into a further series of slices based on the ^{13}C chemical shift of the ^{13}C atoms directly bonded to the aliphatic protons indicated in F_1.

The pulse scheme of the new 4D experiment is shown in Fig. 2. It combines three separate 2D experiments, namely ^1H-^{13}C HMQC, ^1H-^1H NOESY, and ^1H-^{15}N HMQC sequences. Transfer of magnetization between protons and the directly bonded ^{15}N or ^{13}C heteronucleus is achieved by means of multiple quantum coherence (17),

whereas transfer of magnetization between protons occurs by through-space NOE effects. The transfer of magnetization from the aliphatic protons to the NH protons thus follows the pathway:

$$^1H \xrightarrow{^1J_{CH}} {}^{13}C \xrightarrow{^1J_{CH}} {}^1H \xrightarrow{NOE}$$

$$NH \xrightarrow{^1J_{NH}} {}^{15}N \xrightarrow{^1J_{NH}} NH$$

The chemical shifts of ^{13}C, ^1H, and ^{15}N evolve during the variable time periods t_1, t_2, and t_3, which are incremented independently, and the NH signal is acquired during the acquisition period t_4. A 4D Fourier transformation of the resulting data matrix with respect to t_1, t_2, t_3, and t_4 yields a 4D spectrum in which every NOE interaction between an NH proton and an aliphatic proton is determined by four frequency coordinates, the chemical shift values of the two protons involved in the F_2 and F_4 dimensions and the chemical shifts of the ^{13}C and ^{15}N nuclei attached to these two protons in the F_1 and F_3 dimensions, respectively. Signal not originating from an aliphatic proton or terminating on an amide proton is efficiently canceled by appropriate phase cycling of the ^{13}C and ^{15}N pulses, as indicated in the caption to Fig. 2. Three key aspects of practical importance should be noted. The first is that the number of peaks

in this 4D spectrum is the same as that present in the corresponding ^{15}N-^{13}C-edited 3D and 2D spectra. Thus, the extension to four dimensions affords an increase in resolution without a concomitant increase in complexity. Second, the through-bond transfer steps are highly efficient as they involve couplings (90 to 130 Hz) that are much larger than the linewidths. Consequently the sensitivity of the 4D experiment is high. Third, extensive folding is used to maximize resolution in the $^{13}C(F_1)$ dimension (10, 18). As a result, each ^{13}C coordinate corresponds to a series of ^{13}C chemical shifts that, in the present case, are separated by intervals of 20.71 ppm. This process does not complicate the interpretation of the 4D spectrum in any way since all ^{13}C resonances of IL-1β have been assigned (14) and the appropriate ^{13}C chemical shift is readily determined from the ^1H chemical shift of the aliphatic proton from which the magnetization originates (10, 12).

Selected $F_4(NH)$-$F_2(^1H)$ slices of the 4D ^{13}C-^{15}N-edited NOESY experiment of 1.7 mM ^{13}C-^{15}N-labeled IL-1β at two $^{15}N(F_3)$ and several $^{13}C(F_1)$ frequencies are shown in Fig. 3, together with the corresponding $F_3(NH)$-$F_1(^1H)$ slices of the 3D ^{13}C-^{15}N-edited ^1H-^{15}N NOESY-HMQC spectrum at the same $^{15}N(F_2)$ chemical shifts. The 4D
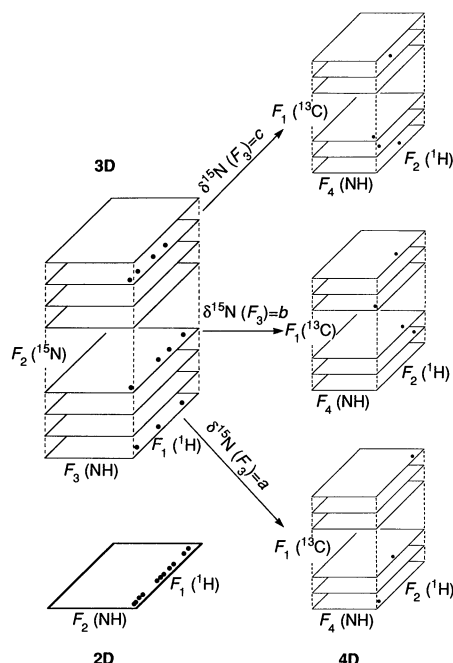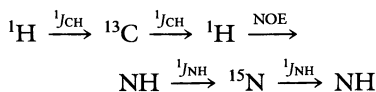

Fig. 1. Schematic illustration of the progression and relation between heteronuclear edited 2D, 3D, and 4D NOESY spectra. The closed circles represent NOE cross peaks between NH and aliphatic protons. In the 2D spectrum, cross peaks from 11 aliphatic protons to 3 NH protons at a single NH chemical shift are indicated. In the 3D spectrum, these peaks are spread into a third dimension according to the chemical shift of the directly bonded ^{15}N atoms. In the illustration the peaks are now located in three distinct planes corresponding to three different ^{15}N chemical shifts, thereby removing the overlap arising from NH chemical shift degeneracy and indicating that the NOEs involve three separate NH protons. Although the NH protons are resolved in the 3D spectrum, the identity of the aliphatic protons can still only be established by their ^1H chemical shifts. In the 4D spectrum, each plane of the 3D spectrum constitutes a cube composed of a series of slices at different ^{13}C chemical shifts. The identity of the originating aliphatic protons can now be established unambiguously as they are characterized by both ^1H and ^{13}C chemical shifts.
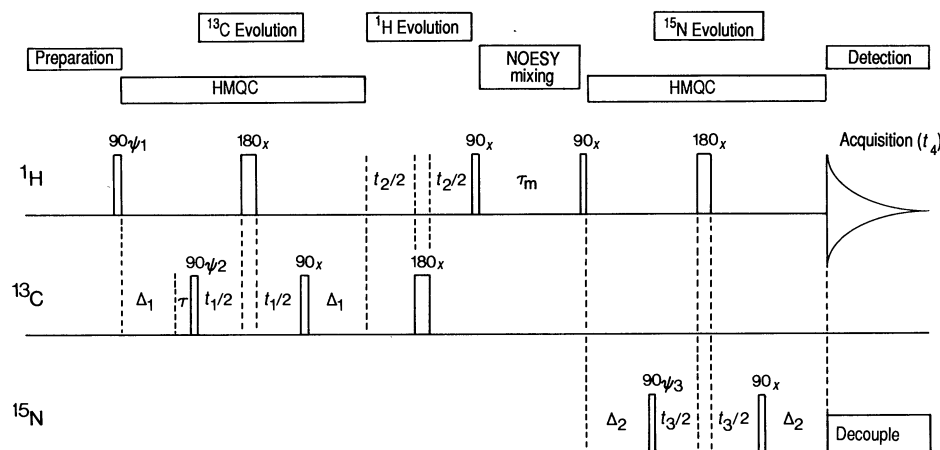

Fig. 2. Pulse sequence of the ^{13}C-^{15}N-edited NOESY 4D experiment. Water suppression is performed during both the relaxation delay and NOE mixing period with an off-resonance DANTE scheme (18). In order to minimize relaxation losses, the delays Δ_1 and Δ_2, which allow for efficient creation of heteronuclear multiple quantum coherence, are set to 3.0 and 4.5 ms, slightly less than $1/(2J_{HC})$ and $1/(2J_{HN})$, respectively. The NOE mixing time τ_m was set to 96 ms. The delay τ immediately prior to application of the first ^{13}C 90° pulse is included to compensate for the ^{13}C 180° pulse so that no first-order phase correction is necessary in F_2. The ^1H, ^{13}C, and ^{15}N carriers were positioned at 8.1, 43.0, and 121.0 ppm, respectively, and ^{13}C and ^{15}N radio frequency (rf) power levels of 16.7 and 1.25 kHz were used for all pulses. WALTZ decoupling (20) was performed during acquisition with a 1.25-kHz rf field. The phase cycling used was: $\psi1 = 4(x)$, $\psi2 = 2(x,-x)$, $\psi3 = 2(x),2(-x)$, and acquisition $= x,-x,-x,x$. Quadrature in the t_1, t_2, and t_3 dimensions was achieved by changing the phases of $\psi1$, $\psi2$, and $\psi3$ by 90° in an independent manner with the States-TPPI method (21). The spectrum was recorded with sequential quadrature detection during the detection period t_4. The experiment was recorded on a Bruker AM-600 spectrometer equipped with a triple-resonance probe optimized for ^1H detection. The acquired 4D data matrix comprised 16 complex (t_1) by 64 complex (t_2) by 16 complex (t_3) by 512 real (t_4) data points. The delays and pulse widths in the sequence were chosen such that the phase of the folded peaks in F_1 is the same as those that are not folded (18). The spectral widths used in F_1, F_2, F_3, and F_4 are 20.71, 8.3, 26.0, and 6.94 ppm, respectively, with corresponding acquisition times of 5.0, 12.6, 9.8, and 61.4 ms in t_1, t_2, t_3, and t_4, respectively.

experiment was recorded in only 6 days, whereas the 3D data set was obtained in 1 day. The two slices of the 3D spectrum at $\delta^{15}N = 118.1$ and 119.8 ppm represent typical planes in the 3D spectrum. The spectral simplification in the 4D slices relative to the 3D ones is obvious. Examination of the two 3D slices reveals a large number of NOEs between NH protons and aliphatic protons resonating between 5.5 and 0 ppm. Those involving intraresidue NH-CαH NOEs can be readily identified by comparison with a 3D ^{1}H-^{15}N HOHAHA-HMQC spectrum [9] in which correlations between NH and aliphatic protons are established through intraresidue scalar $^3J_{HN\alpha}$ couplings. Providing the amino acid sequence is known and some spin systems have been identified, it is also usually possible to assign the sequential CαH(i)-NH(i + 1) NOEs from the 3D spectrum with confidence. The remaining NOEs, and in particular those involving long-range interactions between residues far apart in the sequence, are very difficult and often impossible to interpret in the 3D spectrum because of extreme crowding and overlap of aliphatic ^{1}H resonances. For example, between 1.2 and 0.8 ppm alone, there are 57 separate ^{1}H resonances [14]. Thus, although the destination NH proton can be uniquely defined in the 3D spectrum, there remains a large choice for the identity of the originating aliphatic proton. By spreading out the NOEs between NH and aliphatic protons on the basis of both ^{15}N and ^{13}C chemical shifts in the 4D spectrum, this problem is completely removed, and the specific identification of NOE interactions is reduced to matching all four chemical shifts with a database of complete ^{1}H, ^{13}C, and ^{15}N assignments previously obtained by analysis of a series of 3D heteronuclear double- and triple-resonance spectra [14]. As an example, consider the NOEs between an aliphatic ^{1}H resonance at 0.89 ppm and the NH protons of Ser^{21}, Leu^{27}, Gln^{39}, and Val^{58}. The two NOEs involving Leu^{21}(NH) and Leu^{27}(NH) are seen in the slice at δ^{13}C values of 65.88, 45.17, and 24.46 ppm, whereas those involving Gln^{39}(NH) and Val^{58}(NH) are observed in the slice at δ^{13}C values of 63.25, 42.54, and 21.83 ppm. From the ^{1}H and ^{13}C assignments already in hand, we conclude that the NOEs to Leu^{21}(NH) and Leu^{27}(NH) involve one of the methyl groups of Leu^{26}. The NOEs to Gln^{39}(NH) and Val^{58}(NH) could involve a methyl group of either Val^{19} or Val^{100}. However, the NOE to Val^{58}(NH) is maximal in this slice, whereas that to Gln^{39}(NH) is maximal in the adjacent slice downfield in ^{13}C chemical shift, indicating that they arise from methyl groups with different ^{13}C chemical

shifts. This enables us to deduce that the NOE to Val^{58}(NH) originates from Val^{100}(Cγ^bH$_3$), whereas that to Gln^{39}(NH) is from Val^{19}(Cγ^aH$_3$).

In conclusion, we have demonstrated that ^{13}C-^{15}N–edited 4D NOESY spectroscopy is a powerful and conceptually simple approach for completely removing ambiguities

associated with valuable through-space connectivities between aliphatic and NH protons. Further, the spectra can be obtained with high sensitivity on ~1 to 2 mM ^{15}N-^{13}C–labeled protein samples in a reasonable amount of measuring time. There are two fundamentally different approaches for increasing the resolution in protein NMR
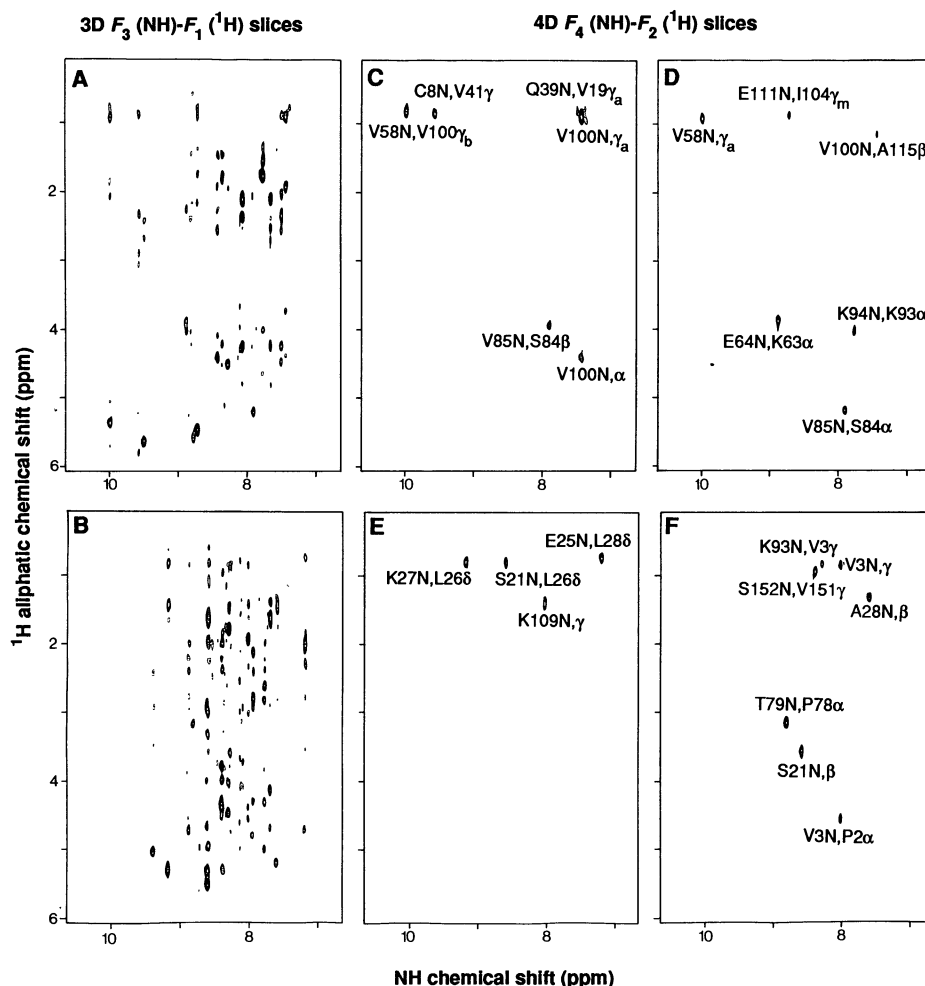

3D F_3 (NH)-F_1 (^{1}H) slices   **4D F_4 (NH)-F_2 (^{1}H) slices**

NH chemical shift (ppm)

Fig. 3. Representative F_4(NH)-F_2(^{1}H) planes of the 4D ^{15}N-^{13}C–edited NOESY spectrum together with the F_3(NH)-F_1(^{1}H) slices of the 3D ^{15}N-^{13}C–edited NOESY spectrum at the corresponding ^{15}N frequencies. Peak assignments were derived on the basis of the complete ^{1}H, ^{15}N, and ^{13}C assignments obtained from the analysis of a variety of 3D heteronuclear double and triple-resonance experiments [14]. The 3D and 4D data sets were processed with an approach described previously [18]. For the 3D slices, the ^{15}N(F_2) values (parts per million) are 118.1 for (**A**) and 119.8 for (**B**). For the 4D slices, the ^{15}N(F_3) values (ppm) are 118.1 for (**C**) and (**D**) and 119.8 for (**E**) and (**F**), and the ^{13}C(F_1) values (ppm) are 63.25, 42.54, and 21.83 for (C), 58.65, 37.94, and 17.23 for (D), 65.88, 45.17, and 24.46 for (E), and 62.59, 41.88, and 21.17 for (F). A time-domain convolution routine [22] was used for both 3D and 4D data sets to remove the baseline distortion arising from the residual water resonance. In the case of the 3D ^{15}N-^{13}C–filtered NOESY data set, a doubly phase shifted sine bell window extending from 60° on the left to 165° on the right-hand side was used prior to transformation in F_2. One zero filling of the data was used in F_2 with double zero filling in the other two dimensions. A simple in-house routine was used for the F_2 Fourier transform whereas commercially available software (NMRi, Syracuse, New York) was used to process the F_1-F_3 planes. Processing of the 4D data set was done in several stages. Initially the data were processed in F_3 with in-house written routines. A doubly shifted sine bell extending from 60° to 165° was used as well as a single zero filling prior to Fourier transformation. After the F_3 transformation, a set of 32 3D data matrices filtered by the ^{15}N chemical shift was generated. Processing of the ^{13}C dimension (F_1) was accomplished next. A doubly shifted sine bell extending from 65° to 170° was used followed by double zero filling and Fourier transformation with software developed in-house. Finally, individual F_2-F_4 planes were processed with commercially available software. The t_3 processing and subsequent transformation required approximately 12 hours on a Sun Sparc workstation, with an additional 1 to 2 hours required for the processing of each of the resultant 32 3D data sets. The final digital resolution in each of the four dimensions was 48.8, 19.5, 49.4, and 4.1 Hz per point in F_1, F_2, F_3, and F_4, respectively.

spectra. The conventional approach improves the resolution in 2D NMR spectra by increasing the digital resolution and by using strong resolution enhancement digital filtering functions at the expense of sensitivity. The new approach presented in this paper improves the resolution by increasing the dimensionality of the spectrum and simultaneously yields important additional information about the system (that is, ^{15}N and ^{13}C chemical shifts). This approach is much less sensitive to wide line widths associated with larger proteins. Indeed, it can easily be calculated that 4D spectra with virtual lack of resonance overlap and good sensitivity can be recorded for proteins as large as 40 kD. Because the resolution in the 4D spectrum shown is limited by digitization, spectra with equivalent resolution can be recorded at magnetic field strengths significantly lower than 600 MHz (14.1 T). Indeed, the inherent resolution of 4D NMR spectroscopy is so high that 4D NMR spectra should be completely analyzable even at low digitization by automated procedures. Finally, we note that the present 4D data set has been processed in only a very coarse manner by Fourier transformation of severely truncated signals. It is expected that spectra of far superior quality could be obtained in much shortened measuring times with more sophisticated data processing algorithms based on linear prediction (19). Indeed, such an approach should open the practical possibility for yet a further increase in dimensionality.

REFERENCES AND NOTES

1. Abbreviations: NMR, nuclear magnetic resonance; NOE, nuclear Overhauser effect; NOESY, nuclear Overhauser enhancement spectroscopy; HMQC, heteronuclear multiple quantum coherence; HOHAHA, homonuclear Hartmann-Hahn; IL-1β, interleukin-1β.
2. G. M. Clore and A. M. Gronenborn, CRC Crit. Rev. Biochem. Mol. Biol. 24, 479 (1989); K. Wüthrich, Acc. Chem. Res. 22, 36 (1989); G. M. Clore and A. M. Gronenborn, Ann. Rev. Biophys. Chem., in press.
3. P. C. Driscoll, A. M. Gronenborn, L. Beress, G. M. Clore, Biochemistry 28, 2188 (1989); P. J. Kraulis et al., ibid., p. 7241; G. M. Clore, E. Appella, M. Yamada, K. Matsushima, A. M. Gronenborn, ibid. 29, 1689 (1990).
4. A. D. Kline, W. Braun, K. Wüthrich, J. Mol. Biol. 204, 675 (1988); Y. Q. Qian et al., Cell 59, 573 (1989).
5. K. Wüthrich, NMR of Proteins (Wiley, New York, 1986); G. M. Clore and A. M. Gronenborn, Prot. Eng. 1, 275 (1987).
6. C. Griesinger, O. W. Sørensen, R. R. Ernst, J. Magn. Reson. 73, 574 (1987); H. Oschkinat et al., Nature 332, 374 (1988).
7. B. H. Oh, W. M. Westler, P. Darba, J. L. Markley, Science 240, 908 (1988).
8. S. W. Fesik and E. R. P. Zuiderweg, J. Magn. Reson. 78, 588 (1988); D. Marion, L. E. Kay, S. W. Sparks, D. A. Torchia, A. Bax, J. Am. Chem. Soc. 111, 1515 (1989); E. R. P. Zuiderweg and S. W. Fesik, Biochemistry 28, 2387 (1989).
9. D. Marion et al., Biochemistry 28, 6150 (1989).
10. L. E. Kay, M. Ikura, A. Bax, J. Am. Chem. Soc. 112, 888 (1989); A. Bax et al., J. Magn. Reson. 86, 620 (1990).
11. S. W. Fesik et al., J. Am. Chem. Soc. 112, 886 (1989).
12. A. Bax, G. M. Clore, A. M. Gronenborn, J. Magn. Reson., in press.
13. L. E. Kay, M. Ikura, R. Tschudin, A. Bax, ibid., in press; M. Ikura, L. E. Kay, A. Bax, Biochemistry 29, 4659 (1990).
14. P. C. Driscoll, G. M. Clore, D. Marion, P. T. Wingfield, A. M. Gronenborn, Biochemistry 29, 3542 (1990); G. M. Clore, A. Bax, P. C. Driscoll, P. T. Wingfield, A. M. Gronenborn, ibid., p. 4668.
15. J. J. Oppenheim, E. J. Kovacs, K. Matsushima, S. K. Durum, Immunol. Today 7, 45 (1986); C. A. Dinarello, Ann. N.Y. Acad. Sci. 546, 122 (1988); M. A. S. Moore, Immunol. Res. 8, 165 (1989).
16. R. R. Ernst, G. Bodenhausen, A. Wokaun, Principles of Nuclear Magnetic Resonance in One and Two Dimensions (Clarendon, Oxford, 1987).
17. L. Mueller, J. Am. Chem. Soc. 101, 4481 (1979); A. Bax, R. H. Griffey, B. L. Hawkins, J. Magn. Reson. 55, 301 (1983).
18. L. E. Kay, D. Marion, A. Bax, J. Magn. Reson. 84, 72 (1989).
19. H. Gesmar and J. J. Led, ibid. 76, 183 (1988).
20. A. J. Shaka, J. Keeler, T. Frenkiel, R. Freeman, ibid. 52, 335 (1983).
21. D. Marion, M. Ikura, R. Tschudin, A. Bax, ibid. 85, 393 (1989).
22. D. Marion, M. Ikura, A. Bax, ibid. 84, 425 (1989).
23. We thank P. Wingfield for preparing the sample of ^{15}N-^{13}C-labeled interleukin-1β and R. Tschudin for valuable technical support. Supported by the Intramural AIDS Antiviral Program of the Office of the Director of the National Institutes of Health (A.M.G., G.M.C., and A.B.). L.E.K. acknowledges a postdoctoral fellowship from the Medical Research Council of Canada and the Alberta Heritage Trust Foundation.

4 April 1990; accepted May 1990

Prevention of Activated Neutrophil Adhesion to Endothelium by Soluble Adhesion Protein GMP140

JENNIFER R. GAMBLE, MICHAEL P. SKINNER, MICHAEL C. BERNDT, MATHEW A. VADAS*

Neutrophils and monocytes, but not lymphocytes, adhered strongly to plastic surfaces coated with GMP140, a protein of endothelial cells and platelets. This adhesion of neutrophils was mediated by GMP140 and not by the CD18 integrin complex. By contrast, GMP140 in solution inhibited the CD18-dependent adhesion of tumor necrosis factor–α–activated neutrophils to plastic surfaces and resting endothelium, but not of resting neutrophils to tumor necrosis factor–α–activated endothelium. Thus, the binding of a soluble form of an adhesion protein selectively inhibited another set of adhesive events. Soluble GMP140 may be important in maintaining the nonadhesiveness of neutrophils in the circulation and may serve to limit inflammatory reactions.

D URING INFLAMMATION, CIRCU- lating blood cells adhere to patches of endothelium and migrate into tissues. This process is regulated by cytokines such as tumor necrosis factor–α (TNF-α) and is mediated by adhesion proteins, some of which belong to the LEC-CAM (lectin–epidermal growth factor–complement binding cell adhesion molecule) family (1). GMP140, a glycoprotein of 140 kD, is present in the alpha granules of platelets and the Weibel Palade bodies of endothelial cells (ECs) (2–4). Analysis of the cDNA suggests three possible forms of GMP140: two transmembrane forms (with complement binding regions of different lengths) and a soluble form, with the transmembrane domain deleted (2). Upon platelet activation or treatment of ECs with thrombin or hista-

mine, the secretory granules are rapidly exocytosed, resulting in a redistribution of transmembrane GMP140 into the plasma membrane (5–7). Endothelial GMP140 has structural similarity to adhesion molecules ELAM-1 (endothelial leukocyte adhesion molecule–1) and MEL-14, which belong to the LEC-CAM family (2, 8, 9). ELAM-1, although not present on resting endothelium, mediates adhesion of neutrophils [polymorphonuclear leukocytes (PMNs)] to endothelium activated by TNF or interleukin-1 (IL-1) (10). MEL-14, present on PMNs and lymphocytes, is involved in lymphocyte homing to high endothelial venules (11). We used platelet GMP140 that was purified to homogeneity (12) to investigate its role in adhesive phenomena, and our data suggest that elaboration or secretion of GMP140 serves to prevent adhesion and the development of inflammatory responses.

GMP140 was coated onto plastic microtiter wells and was adhesive for freshly isolated, nonactivated PMNs and monocytes, but not T lymphocytes (Fig. 1A). Adhesion was concentration-dependent (Fig. 1A), and the

J. R. Gamble and M. A. Vadas, Division of Human Immunology, Institute of Medical and Veterinary Science, Frome Road, Adelaide, South Australia, 5000.
M. P. Skinner and M. C. Berndt, Research Centre for Thrombosis and Cardiovascular Disease, Department of Medicine, Westmead Hospital, New South Wales 2006.

*To whom correspondence should be addressed.